Hindawi
Active and Passive Electronic Components
Volume 2024, Article ID 8722642, 15 pages
https://doi.org/10.1155/2024/8722642

Research Article

Design of a Microwave Quadrature Hybrid Coupler with Harmonic Suppression Using Artificial Neural Networks

Saeed Roshani,[1] **Salah I. Yahya**,[2] **Maher Assaad**,[3] **Muhammad Akmal Chaudhary**,[3] **Fawwaz Hazzazi**,[4] **Yazeed Yasin Ghadi**,[5] **Saeed Mostafaei**,[1] **and Sobhan Roshani**[1]

[1]*Department of Electrical Engineering, Kermanshah Branch, Islamic Azad University, Kermanshah, Iran*
[2]*Department of Communication and Computer Engineering, Cihan University-Erbil, Erbil 44001, Iraq*
[3]*Department of Electrical and Computer Engineering, College of Engineering and Information Technology, Ajman University, Ajman 346, UAE*
[4]*Department of Electrical Engineering, College of Engineering in Al-Kharj, Prince Sattam bin Abdulaziz University, Al Kharj 11492, Saudi Arabia*
[5]*Software Engineering and Computer Science Department, Al Ain University, Al Ain, UAE*

Correspondence should be addressed to Sobhan Roshani; sobhan_roshany@yahoo.ca

Received 3 January 2024; Revised 2 February 2024; Accepted 19 February 2024; Published 11 March 2024

Academic Editor: Yuh-Shyan Hwang

In this paper, a compact and simple structure of an elliptic microstrip lowpass filter (LPF) is designed for harmonic suppression in microwave quadrature hybrid coupler (QHC) applications. A radial resonator and a rectangular resonator are used to produce an elliptic LPF. The proposed LPF is used on the outer sides of the branch line coupler, which has improved the coupler harmonic suppression. Furthermore, artificial neural networks (ANNs) are incorporated to improve the LPF design process. The LPF best structure is obtained using the proposed ANN model. The proposed LPF has a compact size, which only occupies 16.4 mm × 7.3 mm equals to 0.164 λg × 0.073 λg, has a cut frequency of 2.2 GHz, and shows a sharp transmission band with a roll-off rate of 158.3 dB/GHz. Finally, the deigned QHC operates correctly at 1 GHz, which shows high harmonic suppression ability. The proposed QHC provides wide suppression band from 2.25 GHz up to more than 14 GHz, which can effectively suppress 3rd, to 14th harmonics. The proposed coupler features desirable parameters of S_{11}, S_{21}, S_{31}, and S_{41}, with magnitude of −21 dB, −3.4 dB, −3.3 dB, and −22.5 dB, at the operating frequency. The proposed approach mitigates the complexity of the circuit fabrication, compared with the previous methods while achieved desirable performances for the proposed QHC.

1. Introduction

Lowpass filters (LPFs) are devices that permit low-frequency signals to pass while reducing the strength of high-frequency signals. The LPFs are commonly used in microwave and communication systems for the applications, in which the desired low frequency signal should be separated from higher frequencies signals [1]. Several types of filters have been used in microwave circuits, such as active [2] and passive LPFs [3, 4].

On the other hand, couplers are devices that are used to distribute power between different transmission lines or components in communication systems and microwave applications [5]. The couplers enable splitting or combining signals, while maintain the desired properties such as impedance matching, isolation, and power division [6–8]. There are several types of couplers, which are widely used in microwave and communication systems, such as QHCs [9] and rat-race couplers [10]. A QHC is also known as a branch line coupler (BLC). In this type of coupler, the input signal is split into two output signals, while maintaining a phase difference of 90 degrees between the outputs. A QHC consists of four λ/4 transmission lines arranged in a rectangular shape [11].

Recently, there are several approaches that have been used to provide harmonic suppression and rejection band in microwave devices, such as couplers and power dividers. In [12], an electromagnetic bandgap (EBG) technique is used to design a U-shaped microstrip LPF. Circular EBG structure is exploited in this work to flatten the pass band and widen the rejection band. Also, defected ground structure (DGS) is another technique, which have been applied on the ground plane of the filters to improve the device performance [13–16]. In [16], interdigital DGS structures are incorporated to design LPF with 3 GHz cut of frequency, which can provide two transmission zeros for rejection band. DGS structure, meandered lines, and squared resonators are applied in [15] to design a filter with frequency of 2.4 GHz, which can provide five poles; however, the suppression band has not high level of attenuation and the pass band is not flat. The effects of DGS structures on performance of LPFs are investigated in [14], where the results of this work showed that the length of three-pole filter with DGS structure is reduced 67%, compared to the conventional three-pole device. Moreover, a filter with squared DGS structures is presented in [13] in order to obtained high rejection stop-band in the frequency response, which shows 30 dB attenuation level in the suppression band. Hairpin resonators with coupler lines are incorporated in [17] to design an LPF at 2.5 GHz, in which the insertion loss of 20 dB is obtained.

The similar techniques have been considered in the couplers to achieve higher performance in the terms of harmonic suppression and wide rejection band. The EBG and DGS techniques are also used to design couplers and power dividers [18, 19]. The EBG squared units are presented in [18] to design a wide band QHC operating at mm wave applications. Wide isolation and matching band is obtained in [18] with the presented unit cells. A planar coupler is presented in [20] using E-shape impedance transformer for dual-band functionality. Dual-band operation is achieved in this device using closed-form design equations based on ABCD matrices [20]. In [21], the folded transmission lines and coupled lines are incorporated to design a dual-band QHC with compact structure. This coupler operates at 1 GHz and 2 GHz and features compact size, compared to the conventional coupler [21]. Using open stubs [6, 22] and different shaped resonators [7] are also common techniques for obtaining rejection band in the couplers and power dividers. Each open stub can provide a transmission zero, which its frequency is dependent on its length [23]. In [24], four open stubs are used in middle of the QHC main branches to obtain rejection band for the designed device, which operates at 0.9 and 2 GHz frequencies. Also, optical couplers have been presented [25] for higher frequencies using crystal photonic structures [26–28].

The presented BLC in [29] integrates open stubs and resonators to achieve enhanced performance, which can suppress unwanted harmonics. A dual-band BLC featuring a wide rejection band for harmonics is developed in [30], operating at 2.6 and 4 GHz. This design incorporates four low-pass filters and four open-ended stubs to enable dual frequencies and reject harmonics at higher frequencies. In [31], a technique is presented for swiftly redesigning miniaturized microstrip couplers to accommodate various operating conditions and dielectric substrate material properties. This dimension scaling method relies on pre-optimized reference designs derived from an equivalent circuit model of the coupler. This approach facilitates scaling across a broad range of operating conditions and substrate parameters. A BLC characterized by compact dimensions and effective harmonic suppression achieved through nonperiodic reactively loaded artificial lines is presented in [32]. These lines incorporate step impedance shunt stubs (SISSs) as reactive loading elements, which introduce transmission zeros crucial for mitigating harmonic interference. Additionally, the reactive loading imparts a desirable slow wave effect to the artificial lines, facilitating device miniaturization [32].

In addition, the applications of artificial neural network (ANN) and artificial intelligence (AI) models have become prevalent in solving engineering challenges [33–36]. Machine learning and optimization strategies have introduced as potential techniques for dealing with several problems [37–41]. Through the training of ANNs on data collected from complicated systems, the underlying behaviors can be captured, facilitating precise predictions and refined control over these systems [42–44]. AI tools have been also widely used in designing of electronics and microwave devices, such as antennas, couplers, and power dividers [8, 45–47].

As mentioned, and explained in the literature, all of the previous approaches have used additional process, such as EBG and DGS structures or used extra resonators, which complicates the coupler structure. In this paper, simple elliptic LPFs are designed and optimized using neural networks. Then, the proposed filters are used in the conventional QHC structure to improve the features of the device. According to the obtained results, the proposed approach has improved the obtained performance of the coupler significantly.

2. The Proposed LPF Design Steps

A rectangular-shaped and a radial-shaped resonator are used to design the proposed LPF. Also, neural network approach has been exploited to design the device with high performances. The structure and frequency responses of different square shaped resonators are investigated, as shown in Figure 1. As result shown, the middle high-impedance line can be used to improve the resonator response and sharpen the transition band. As seen in Figure 1, three steps to create the basic LPF are shown. In Figure 1(a), simple high-low impedance resonators are used to shape a simple filter. In this structure, the length of the high-impedance line is too short. The frequency response of this simple filter is depicted in Figure 1(b), which has a 3.3 GHz cut off frequency and provides a transmission zero at 6.7 GHz. In this structure, the length of the high-impedance line is too short, which this length is increased for the performance improvement, as shown Figure1(c). The frequency response of this LPF is depicted in Figure 1(d), which has a 2.24 GHz cut off frequency and provides a transmission zero at 2.9 GHz. As result shown, this filter has better performance, compared

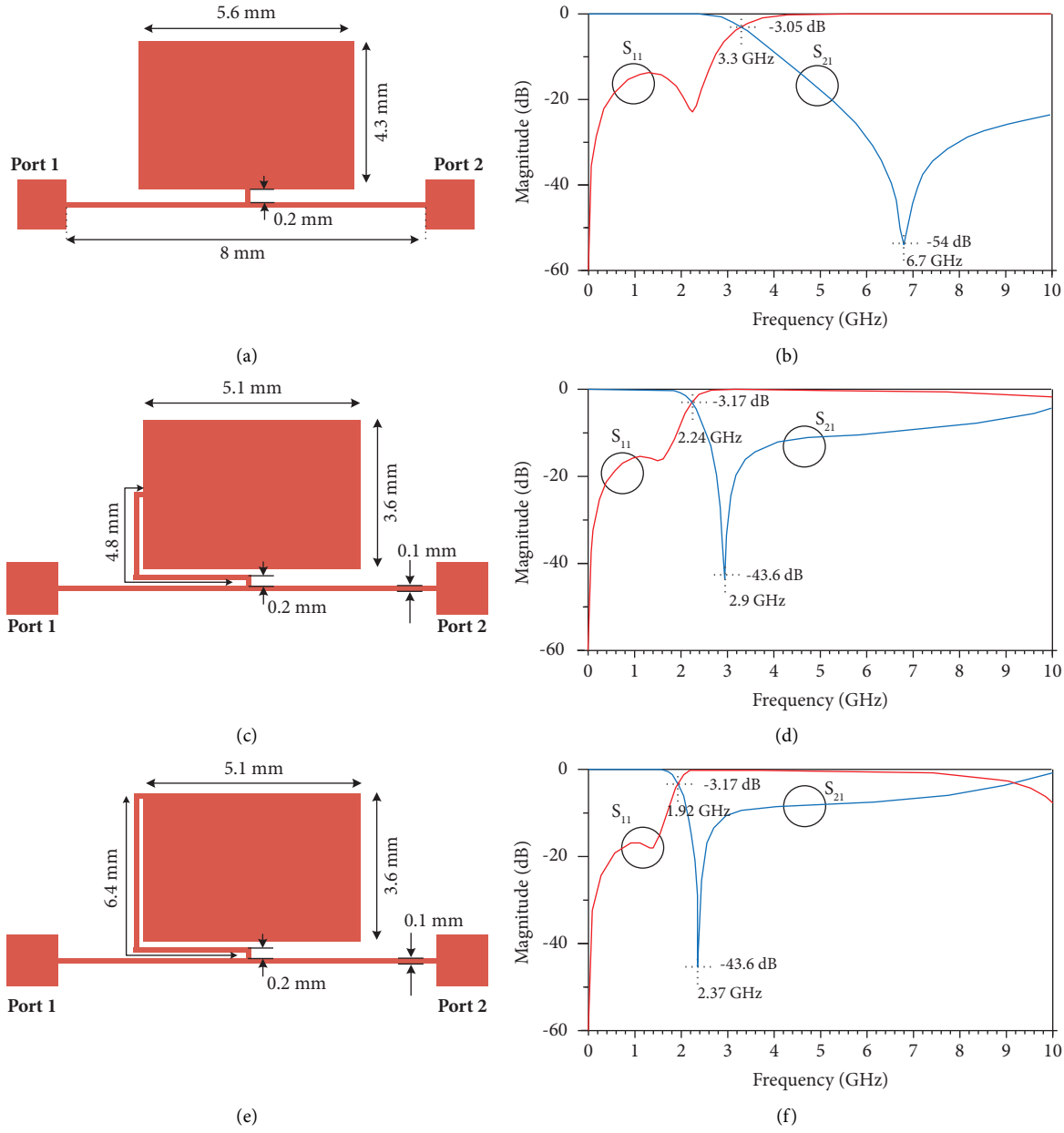

Figure 1: Three steps of creating the basic LPF. (a) The initial structure of the basic LPF. (b) The frequency response for the LPF in step 1, in which the basic LPF only consists of an open-stub and a high impedance line located in a T-shaped structure. The structures and frequency responses for the designed basic LPF in step 2 and step 3 are shown in subfigures (c)–(f). In steps 2 and 3, the middle high impedance line is bended, resulted in size reduction and also performance improvement of the LPF.

with the depicted structure in Figure 1(a). To further improvement, the length of this high-impedance line is increased again as depicted in Figure 1(e). The bended lines are used to reduce circuit size, such that all these three structures occupied same size. The frequency response of the proposed basic LPF with rectangular resonators is depicted in Figure 1(f), which has 1.92 GHz cut off frequency and provides a transmission zero at 2.37 GHz, which has the best performance compared with other depicted filters. All simulations in this paper are executed using momentum and schematic environments of ADS (advanced design system) software.

2.1. LPF Design Steps Using Neural Networks. The basic structure of the proposed elliptic LPF incorporated with rectangular-shaped and radial-shaped resonators is depicted in Figure 2. As shown, the parameters of L1, L2, W1, W2, and D1 are considered to improve the performance of the presented elliptic filter.

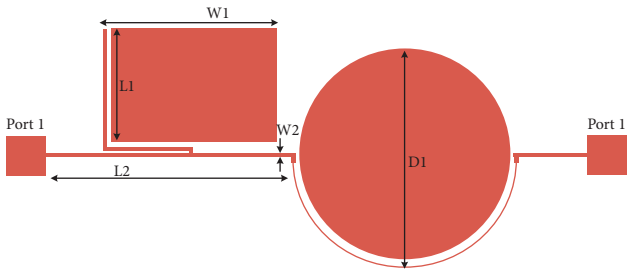

Figure 2: The basic structure of the proposed elliptic LPF incorporated with rectangular-shaped and radial-shaped resonators.

The mentioned parameters of L1, L2, W1, W2, and D1 will be set as the neural network inputs, while the important parameters of elliptic LPF, which are cut-off frequency, fc (GHz), bandwidth, BW (GHz), suppression factor, SF (dB), and roll-off rate, Ro (ζ dB/GHz), will be assumed as the ANN model outputs. The presented model incorporates a multi-layer feedforward ANN capable of forecasting the filter parameters by taking into account the input parameters. This presented model functions as a predictor tool for the presented elliptic filter. Figure 3 illustrates the architecture of the applied multi-layer perceptron (MLP) network, which is a feed forward ANN. As depicted in the figure, the input nodes are connected to the outputs through two hidden layers, which each layer containing five neurons. Sigmoid activation function (Tansig) is used in the hidden layers, while the linear activation function (Purelin) is used at the output of the presented model.

In comparison with the traditional optimization methods, it should be noted that the ANNs do not require equations for modeling. In contrast, optimization methods rely on equations, and in complex structures, it may be challenging to extract all the necessary equations. Optimization methods often require a predefined mathematical model of the system, which may not accurately represent the real-world complexity of certain problems, while ANNs are data-driven models that adapt to the patterns present in the training data. They can handle situations where the underlying system is not well understood or described by a clear mathematical formulation.

In addition, many optimization techniques assume linear relationships between input parameters and output responses. In cases where the relationships are nonlinear, traditional methods may struggle to accurately model and optimize the system, while ANNs are appropriate for tasks where complex dependencies exist between input and output variable. Moreover, the complexity of the design problem with intricate relationships between input parameters and output performance metrics makes ANNs well-suited for capturing and optimizing these relationships. Additionally, the flexibility of ANNs in handling nonlinearities provides a valuable tool in scenarios where traditional optimization methods may fall short.

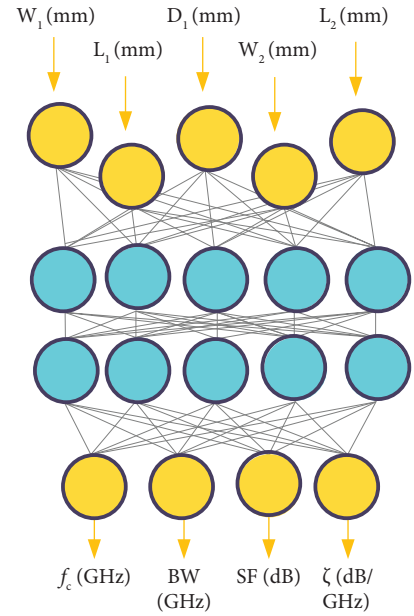

Figure 3: The presented ANN model architecture.

The data used for training and testing procedures of the presented ANN model is listed in Table 1. As seen, the important parameters of L1, L2, W1, W2, and D1, which are depicted in Figure 2, are assumed as input parameters and impact of these parameters on the outputs parameters like cut off frequency, bandwidth, suppression factor level, and sharpness are investigated. Among the 33 samples of data set, first 27 samples are selected for training procedure, the next 5 samples are selected for test procedure, and the last sample is considered as the verification sample.

In Figure 4, predicted and real values of the output parameters of cut-off frequency, *fc* (GHz), bandwidth, BW(GHz), suppression factor, SF(dB), and roll-off rate, Ro (ζ dB/GHz), are depicted. As can be concluded from this figure, the important output parameters of the filter are predicted successfully and the predicted values are close to the real values. So, the proposed model can be used to design and optimize the proposed elliptic filter. In Figure 4, the performance of the proposed model can be analyzed. In regression plots, the relationship between the input variables and the predicted output values can be seen, in both training and testing procedures. The obtained regression plots show that the model can effectively generalize to unseen data and make accurate predictions. In Figure 5, mean square error (MSE) of the fc (GHz), BW (GHz), SF(dB), and Ro (ζ dB/GHz) output parameters in train process of the presented model are shown. As seen, the MSE decreases as the proposed model iteratively adjusts its weights and biases to minimize prediction errors on the training data, which shows that the proposed model is converging towards optimal parameter values. Also, the rapid decrease in MSE plots of fc and Ro parameters shows effective learning in training process of these two parameters.

Table 1: Data used for training and testing procedures of the presented ANN model.

#	Input					Output			
	W1 (mm)	L1 (mm)	D1 (mm)	W2 (mm)	L2 (mm)	Fc (GHz)	BW (GHz)	SF (dB)	Ro (ζ) (dB/GHz)
1	5.1	3.6	6.6	0.1	7.4	2.04	10.31	20	119.3
2	5.1	3.6	6.4	0.1	7.4	2.042	10.17	20	120.8
3	5.1	3.6	6.2	0.1	7.4	2.045	10.481	18.5	115
4	5.1	3.6	6	0.1	7.4	2.047	10.531	18	120.9
5	4.8	3.6	6	0.1	7.4	2.103	10.507	19	114.9
6	4.6	3.6	6	0.1	7.4	2.130	10.3	20	105.7
7	4.0	3.2	5.7	0.2	7.6	2.5	8.45	18.5	93.5
8	4.4	3.8	6	0.1	7.4	2.134	10.22	19.5	113.5
9	4.4	4.0	6	0.1	7.4	2.05	10.40	18.5	117.8
10	4.4	4.2	6	0.1	7.4	1.96	10.30	17	147.3
11	4.6	4.2	6	0.1	7.4	1.926	10.34	16	126.7
12	4.6	4.2	6	0.1	7.6	1.903	10.343	16	117.4
13	4.6	4.2	6	0.1	7.8	1.894	10.21	16.5	144.17
14	4.6	4.2	6	0.1	8.0	1.890	10.19	17	145.9
15	4.6	4.2	6.2	0.1	8.0	1.903	10.51	17	148.2
16	4.6	4.2	6.4	0.1	8.0	1.910	10.46	17.5	148.1
17	4.6	4.2	6.6	0.1	8.0	1.913	10.30	18.5	155.1
18	4.6	4.2	6.5	0.2	8.0	1.911	9.21	14	133.1
19	4.6	4.2	6.3	0.2	8.0	1.902	9.26	13.5	128.9
20	4.6	4.2	6.1	0.2	8.0	1.876	9.479	12	118.2
21	4.6	4.2	6.1	0.2	7.8	1.879	9.659	12	117.8
22	4.6	4.2	6.1	0.2	7.6	1.881	9.781	11.5	118.1
23	4.6	4.0	6.1	0.2	7.6	1.965	9.65	13	120.5
24	4.8	4.0	6.1	0.2	7.6	1.913	9.9	12	122.1
25	4.4	4.0	6.1	0.2	7.6	2.03	9.76	14	153.6
26	4.4	3.8	6.1	0.2	7.6	2.11	9.67	15	146.8
27	4.4	3.6	6.1	0.2	7.6	2.21	9.38	16	151.6
28	4.2	3.6	6.1	0.2	7.6	2.249	9.11	16.5	152.1
29	4.2	3.4	6.1	0.2	7.6	2.33	8.97	17.5	112.1
30	4.0	3.4	6.1	0.2	7.6	2.40	8.69	18.5	102.7
31	4.0	3.2	6.1	0.2	7.6	2.47	5.70	20	90.2
32	4.0	3.2	5.9	0.2	7.6	2.49	7.95	20	94.8
33	4.4	3.6	6	0.1	7.4	2.20	10.24	20	158.3

The calculated errors of the presented ANN model are listed in Table 2, which shows acceptable performance of the proposed model. As results show, the proposed model can predict the resonator performance, precisely. So, the best performance predicted by ANN can be used to design the resonator with optimized performances. According to the ANN model, best performance of the presented LPF is obtained for W1 = 4.4 mm, L1 = 3.6 mm, D1 = 6 mm, W2 = 0.2 mm and L2 = 7.4 mm. These circuit parameters extracted from the proposed ANN model, used to design the resonator with best performance. The frequency response of the final proposed elliptic filter, with the obtained dimensions from ANN, are illustrated in Figure 6. As results shown the proposed device has cut-off frequency of 2.2 GHz, stop-band bandwidth of 10.24 GHz with more than 20 dB suppression level. The proposed LPF provides very sharp response of 158.3 dB/GHz.

The transition band sharpness which also called, roll-off rate, is written in equation (1) as follows:

$$\zeta = \frac{\alpha_{\max} - \alpha_{\min}}{f_s - f_c}\left(\frac{\mathrm{dB}}{\mathrm{GHz}}\right). \quad (1)$$

In equation (1), the minimum and maximum values of α represent 3 dB and 60 dB attenuation levels, respectively, with the corresponding frequencies of f_c and f_s. The roll-off rate value is calculated as 158.3 dB/GHz with corresponding frequencies of f_c and f_s equal to 2.2 GHz to 2.56 GHz.

Moreover, suppression factor of an LPF, which is also known as stopband attenuation, refers to the level of attenuation that the low-pass filter applies to frequencies beyond its cutoff frequency. Typically, the suppression factor is expressed in decibels (dB) and indicates the ratio of the strength of the unwanted signal (higher frequencies) to the strength of the desired signal (lower frequencies). A higher suppression factor means that the filter can attenuate the unwanted frequencies more effectively, resulting in better signal quality.

Figure 7 shows current distribution of the proposed elliptic LPF including a rectangular and a radial resonator. The rectangular resonator exhibits concentrated currents along its edges, emphasizing the resonator role in confining and guiding the electrical energy through the filter. The radial resonator demonstrates a more diffuse and outwardly propagating current distribution,

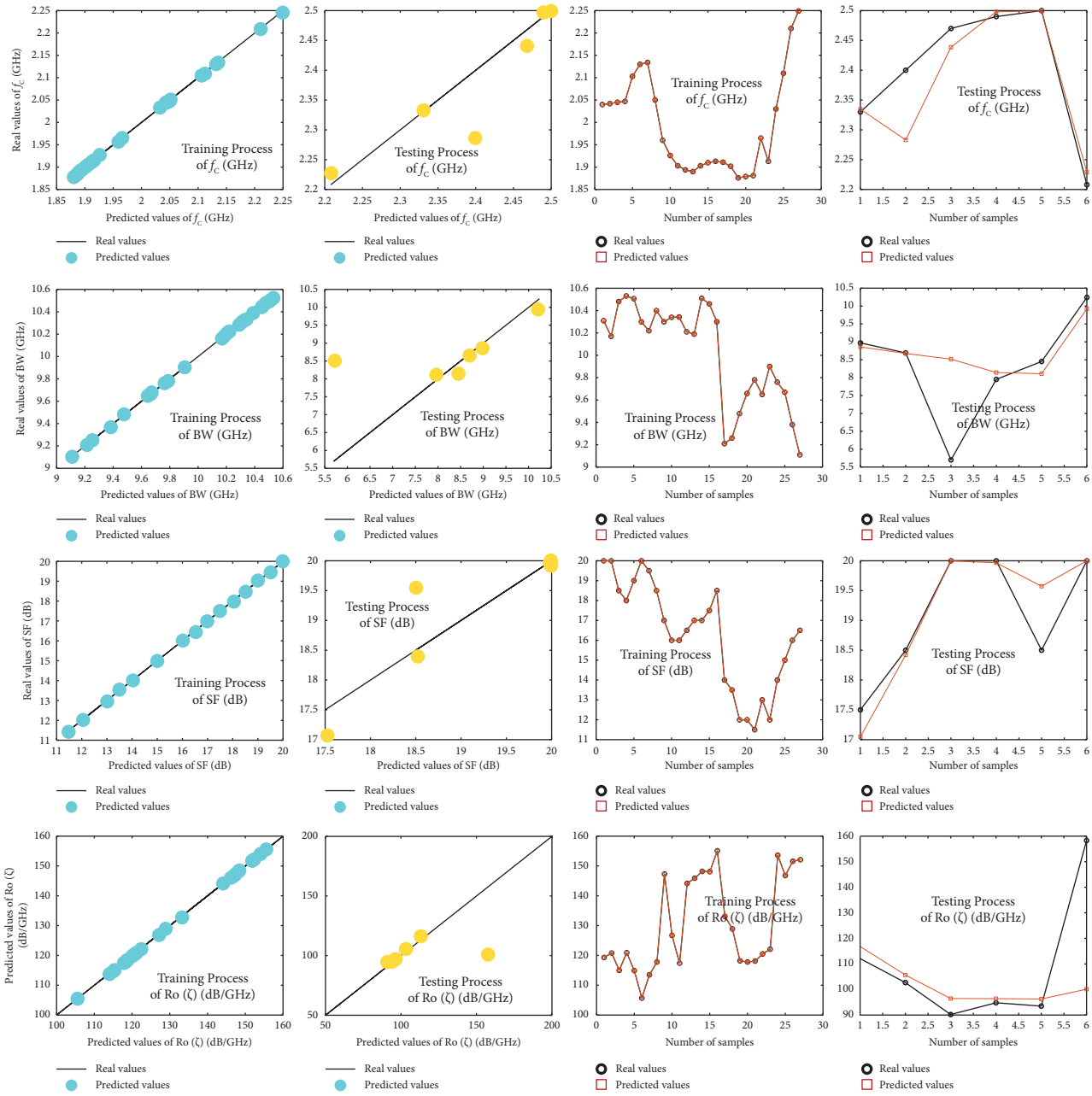

FIGURE 4: Predicted and real values of the output parameters of cut-off frequency, fc (GHz), bandwidth, BW (GHz), suppression factor, SF (dB), and roll-off rate Ro (ζ dB/GHz). In each row of subfigures, the first and second figures are corresponding to the obtained regression from ANN model, where the third and fourth figures representing the predicted output values using ANN model versus number of samplers. The first, second, third, and fourth rows of figures are respectively corresponding to fc (GHz), BW (GHz), SF (dB), and Ro (ζ dB/GHz) output parameters.

highlighting the radial resonator capability to efficiently couple with incoming signals. This visual representation effectively shows the key principles of current distribution within LPF filters, providing valuable insights for filter design.

The LC equivalent circuit and its S-parameters for the presented elliptic LPF is extracted as shown in Figure 8. Two transmission zeroes are provided near 3 GHz and 9 GHz, which have provided wide suppression band. The values of l_{O1} and l_{O2} have the most effects on the 9 GHz and 3 GHz transmission zeros, respectively.

The provided LC circuit is analyzed for better investigation of the filter behavior. As seen the value of seen impedance from two points are shown with Z_A and Z_B, which extracted in equations (2)–(4).

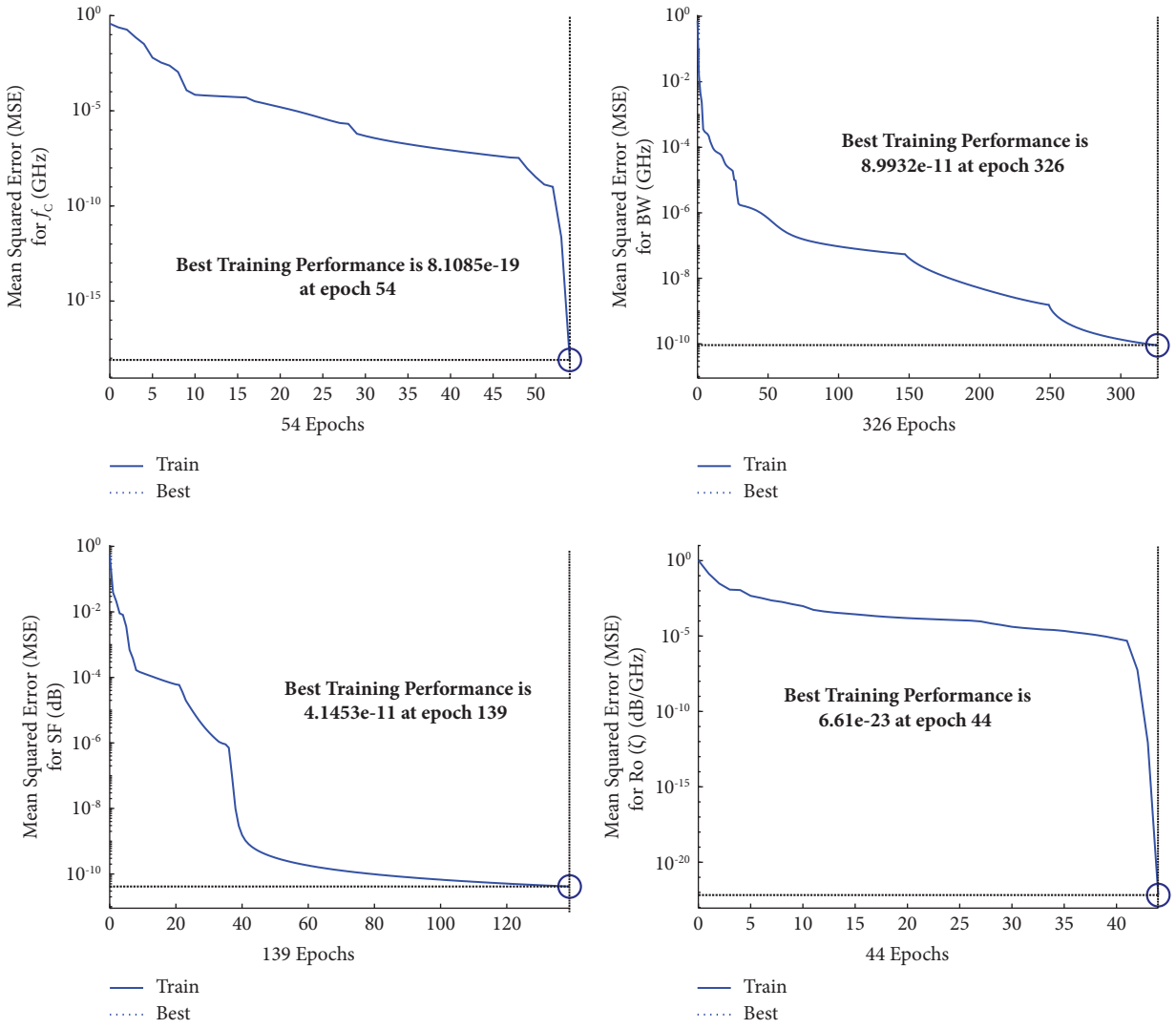

Figure 5: Mean square error (MSE) of the fc (GHz), BW (GHz), SF (dB), and Ro (ζ dB/GHz) output parameters in train process of the presented ANN model.

$$Z_A = \frac{\left((1/\mathrm{Co}_2 S) + \mathrm{Lo}_2 S\right)\left(Z_0 + L_3 S\right)}{Z_0 + (1/\mathrm{Co}_2 S) + L_3 S + \mathrm{Lo}_2 S}, \tag{2}$$

$$Z_B = \frac{\left((1/\mathrm{Co}_1 S) + \mathrm{Lo}_1 S\right)\left(L_2 S + \zeta_1\right)}{(1/\mathrm{Co}_1 S) + L_2 S + \mathrm{Lo}_1 S + \zeta_1}, \tag{3}$$

$$\zeta_1 = \frac{\left((1/\mathrm{Co}_2 S) + \mathrm{Lo}_2 S\right)\left(Z_0 + L_3 S\right)}{Z_0 + (1/\mathrm{Co}_2 S) + L_3 S + \mathrm{Lo}_2 S}. \tag{4}$$

After calculating Z_A and Z_B, the transfer function of the elliptic filter can be achieved as written in equation.

$$H(S) = \frac{Z_0\left((1/\mathrm{Co}_1 S) + \mathrm{Lo}_1 S\right)\left((1/\mathrm{Co}_2 S) + \mathrm{Lo}_2 S\right)}{\left(L_1 S + \left(\left((1/\mathrm{Co}_1 S) + \mathrm{Lo}_1 S\right)\left(L_2 S + \sigma_2\right)/\sigma_1\right)\right)\sigma_1\left(Z_0 + (1/\mathrm{Co}_2 S) + L_3 S + \mathrm{Lo}_2 S\right)}. \tag{5}$$

The parameters of σ_1 and σ_2, which are defined in equations (6) and (7).

Table 2: The calculated errors of the presented ANN model.

	f_c (GHz) errors		BW (MHz) errors		SF (dB) errors		Ro (ζ) (dB/GHz)	
	Train	Test	Train	Test	Train	Test	Train	Test
MRE	1.21×10^{-9}	0.0127	8.74×10^{-5}	0.1006	9.96×10^{-9}	0.0150	2.78×10^{-10}	0.0925
RMSE	3.21×10^{-9}	0.0503	4.54×10^{-5}	1.1690	1.86×10^{-7}	0.4766	7.09×10^{-8}	24.03

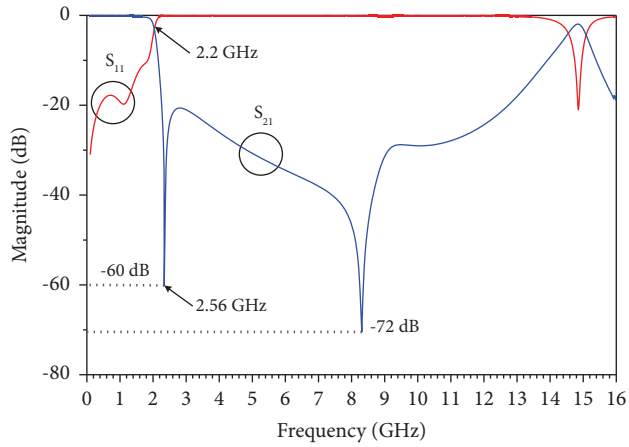

Figure 6: The frequency response of the final proposed elliptic LPF incorporated with radial-shaped and rectangular-shaped resonators.

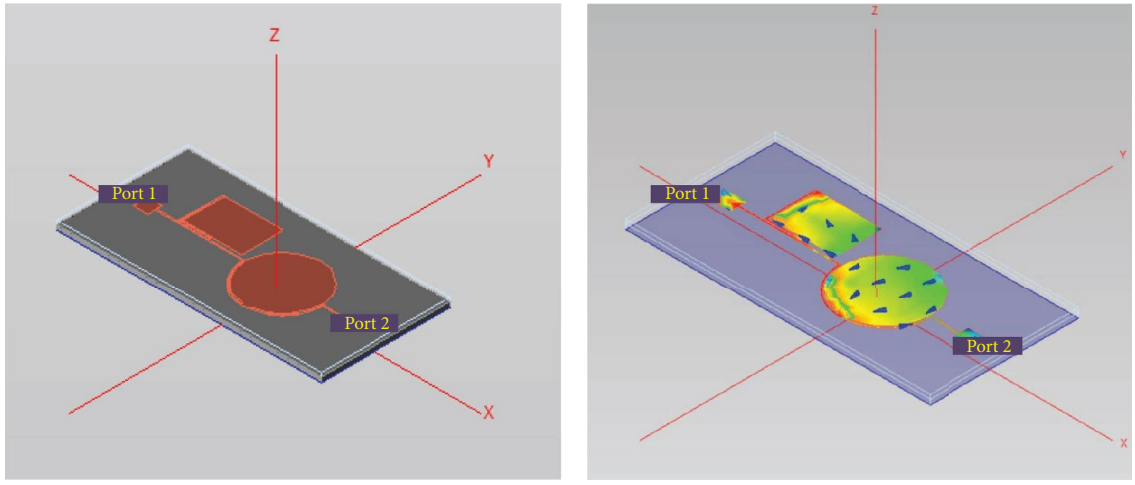

(a) (b)

Figure 7: The (a) 3D structure and (b) current distribution of the proposed elliptic LPF. In the rectangular resonator, the current distribution occurs along the edges of the patch. Also, in the circular resonators, the current distribution is concentrated around the perimeter of the circular structure. The high impedance line ensures that the signal paths remain separate, allowing the LPF to effectively filter out high-frequency components, while allowing low-frequency signals to pass through from input to output.

$$\sigma_1 = \frac{1}{\mathrm{Co}_1 S} + L_2 S + \mathrm{Lo}_1 S + \sigma_2, \tag{6}$$

$$\sigma_2 = \frac{\left((1/\mathrm{Co}_2 S) + \mathrm{Lo}_2 S\right)\left(Z_0 + L_3 S\right)}{Z_0 + \left(1/\mathrm{Co}_2 S\right) + L_3 S + \mathrm{Lo}_2 S}. \tag{7}$$

After finding the transfer function of the presented elliptic filter, the frequency representation of the transfer function can be drawn as shown in Figure 8(c). As shown, the frequency response of the transfer function, obtained from analyses, verifies the simulation results.

3. The Proposed Coupler Design and Results

In this section it will be explained that how the designed elliptic filter is incorporated in the proposed QHC structure to improve the performance of the coupler and also to

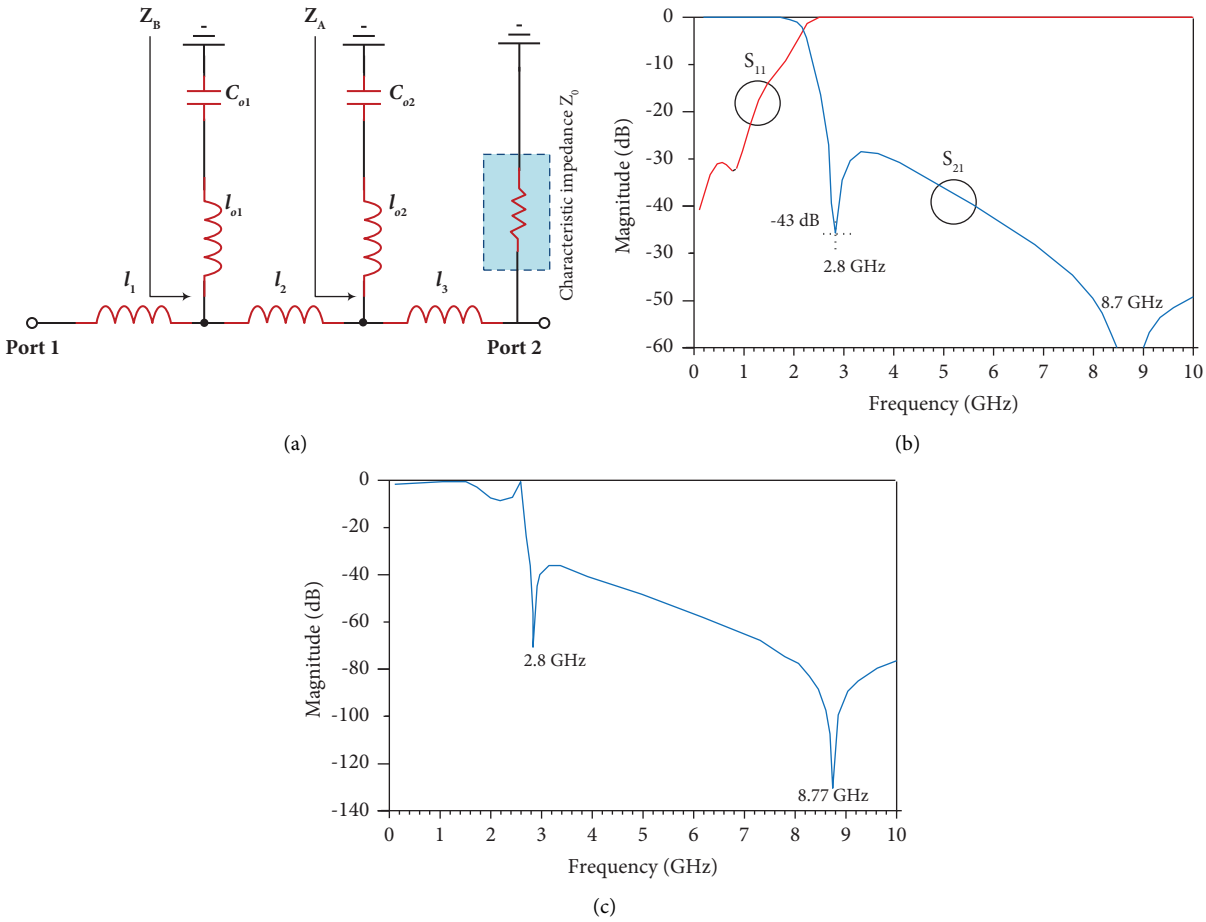

FIGURE 8: The (a) LC equivalent circuit of the designed elliptic LPF. (b) The S-parameters for the presented elliptic LPF, which is obtained by simulation of the LC equivalent circuit. (c) The frequency response of the presented elliptic filter, extracted from analyses, according to equation (5).

provide the filtering response and harmonic suppression ability for the coupler. At the first step the conventional QHC is briefly investigated as explained in the next subsection.

3.1. Conventional QHC Design. A conventional QHC is a specific type of microwave coupler that is commonly used in various applications. The design of a coupler typically involves four microstrip or stripline branches, and the S-parameters for such a coupler should exhibit specific characteristics to ensure its proper operation. Ideally, the S_{11}, reflection coefficient at port one, should be as close to zero as possible, indicating minimal signal reflection at port one. This ensures that most of the input signal is efficiently coupled into the output ports and that there is little energy reflected back to the source. Also, theoretically, the S_{21}, and S_{31}, transmission coefficients from port 1 to port 2, and port 2 to port 3, should be as close to −3 dB (0.707) as possible. A value of −3 dB indicates that half of the input power is transferred to Port 2, while the other half continues to Port 3. Moreover, the S_{41}, transmission coefficient from Port 1 to Port 4, typically represents the isolation between Port 1 and Port 4. Ideally, S_{41} should be as close to zero as possible, indicating that there is minimal direct coupling between these ports. The structure and simulated frequency response of a conventional QHC operating at the frequency of 1 GHz is illustrated in Figure 9. The results show that the frequency response of the simulated conventional QHC is close to ideal one which verifies the design.

3.2. Proposed Coupler Design. The harmonics presence in the frequency response is a common problem in QHC devices. Harmonics are unwanted signal components that occur at integer multiples of the main frequency. The presence of harmonics in the frequency response can be result of nonlinearities in the circuit, and they can degrade the performance of the overall circuit in various ways. As mentioned in the proposed approach, elliptic filter is proposed to mitigate the undesirable issue of harmonics in the QHC by incorporating the filter into the coupler structure. By designing the elliptic filter to have a wide stopband that encompasses the harmonic frequencies of interest, it can effectively attenuate these harmonics. This approach reduces the harmonic content in the output signal of the QHC. The basic circuit structure of the proposed QHC and its simulated frequency response is shown in Figure 10. As seen, the obtained magnitudes of S_{11}, S_{21}, S_{31}, and S_{41}, are −25 dB, −3.15 dB, −3.05 dB, and −19.5 dB respectively, which are

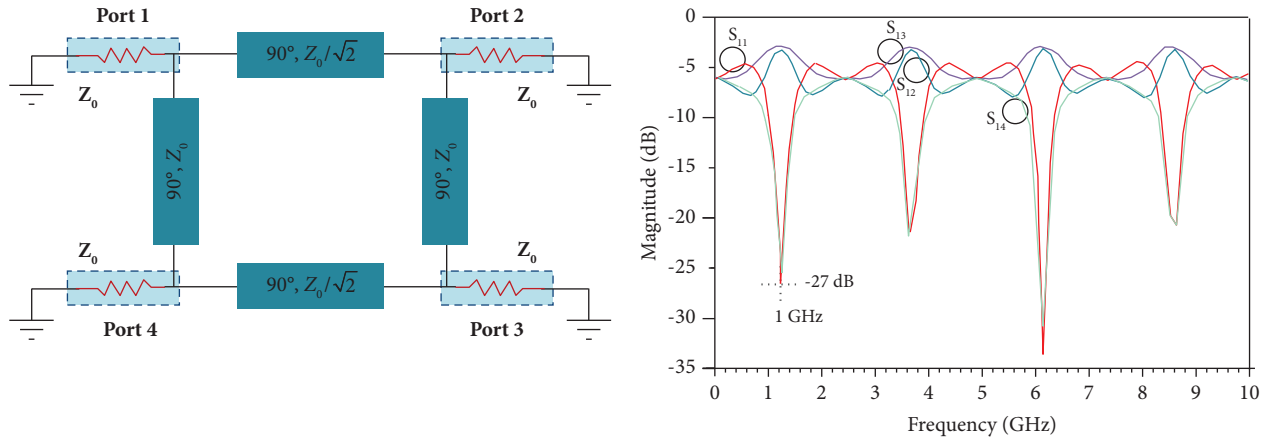

(a) (b)

Figure 9: The (a) structure and (b) simulated frequency response of a conventional QHC operating at the frequency of 1 GHz.

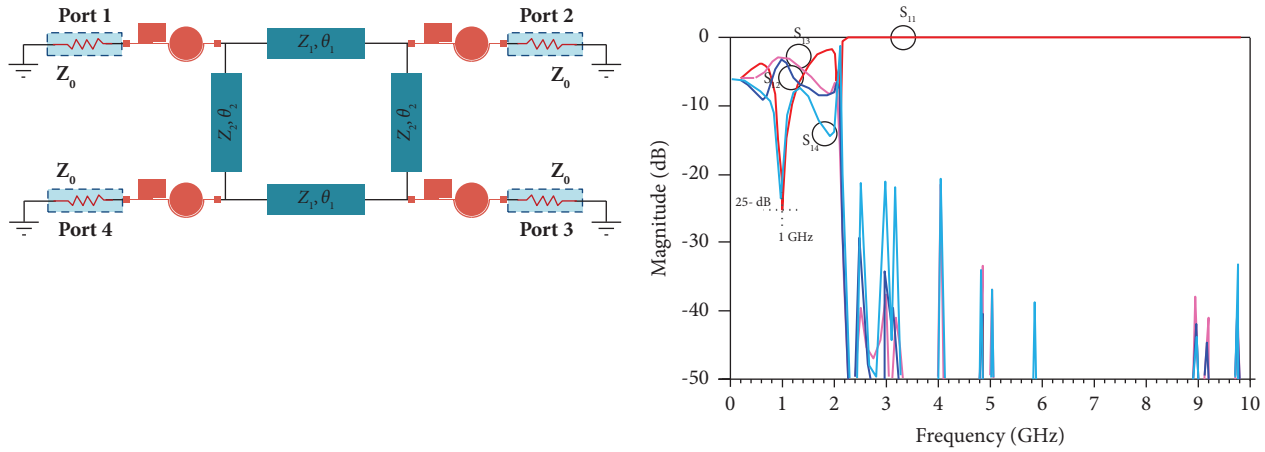

(a) (b)

Figure 10: The basic (a) circuit structure of the proposed QHC and (b) its simulated frequency response.

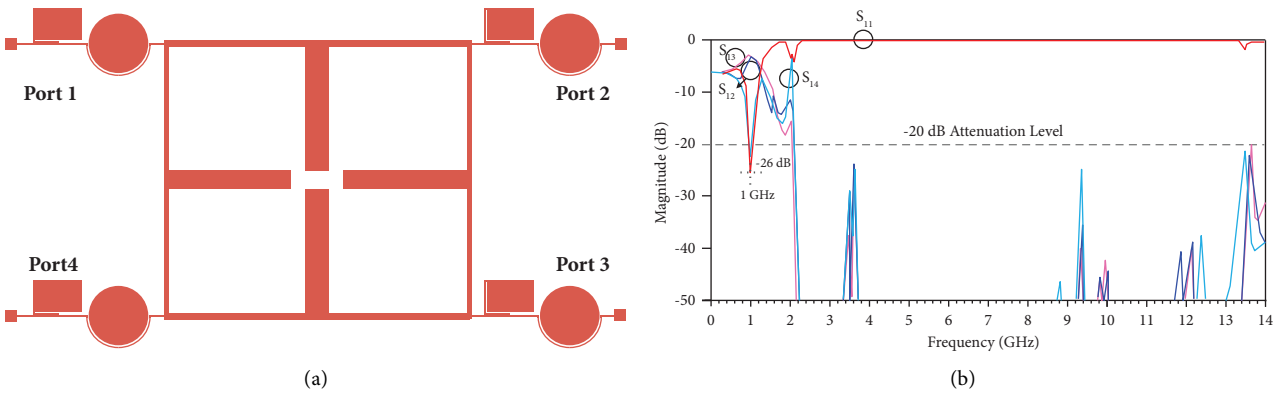

(a) (b)

Figure 11: The (a) layout structure of the proposed QHC and (b) its simulated frequency response.

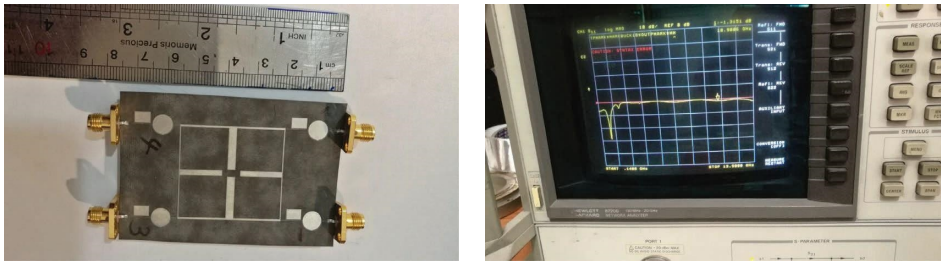

(a) (b)

Figure 12: The (a) fabricated prototype the proposed QHC and (b) the measured frequency response.

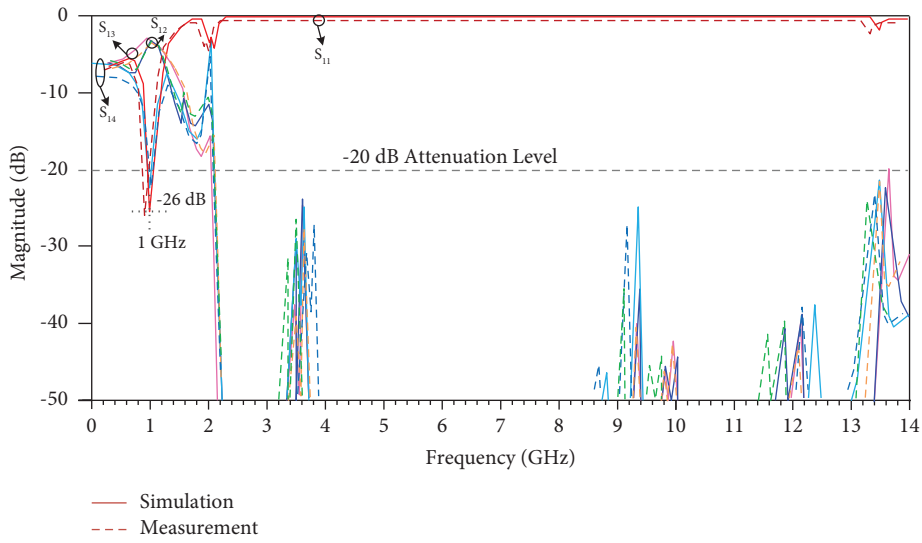

Figure 13: The simulated and measured frequency response of the proposed coupler.

very close to ideal QHC results. Also there is a suppression band from 2.25 GHz up to more than 14 GHz, which can effectively provide a desirable harmonic suppression for the designed QHC.

After circuit simulation and obtaining the desired results, the layout of the proposed coupler is simulated, which the results are shown in Figure 11. The obtained magnitudes of S_{11}, S_{21}, S_{31}, and S_{41}, are −26.1 dB, −3.06 dB, −3.07 dB, and −23.1 dB respectively, for the simulated layout of the proposed QHC. A suppression band of 2.25 GHz up 14 GHz is achieved according to the layout simulation results, which can effectively provide a desirable harmonic suppression for 3^{rd} to 14^{th} harmonics.

A fabricated prototype the proposed QHC and the measured frequency response are shown in Figure 12. The device is simulated and fabricated with RTduroid 5880 substrate and ε_r of 2.2 and the fabricated prototype is measured using 8720B network analyzer. The simulated and measured frequency response of the presented coupler is compared in Figure 13. A good agreement can be seen between the experimental results and simulation data. The obtained magnitudes of S_{11}, S_{21}, S_{31}, and S_{41}, are −21 dB, −3.4 dB, −3.3 dB, and −22.5 dB respectively, for the measured layout of the proposed QHC. The bandwidth of the proposed BLC is 300 MHz, considering 10 dB attenuation for isolation and return loss. This bandwidth starts from 800 MHz up to 1100 MHz, which shows more than 31% of bandwidth.

The performance results of the proposed coupler are compared with similar works and listed in Table 3. The results show the superior performance of the proposed coupler. A wide suppression band from 2.2 GHz up to 14 GHz is obtained for the proposed QHC which can provide 3^{rd} and 14^{th} harmonic suppression. Also, the other

Table 3: Performance summary of the presented coupler and similar works.

Refs.	Frequency (GHz)	Harmonics suppression	Isolation (dB)	Return loss (dB)	Insertion loss (dB)	Type	Applied technique
[8]	1	2^{nd} to 5^{th}	19	18	0.2	Coupler	Open ended resonator
[48]	1.8	2^{nd} and 3^{rd}	20	20	0.6	Power divider	EBG
[49]	1	3^{rd} to 5^{th}	30	30	0.2	Power divider	Capacitor loading
[50]	2.4	2^{nd} and 3^{rd}	20	22	0.65	Power divider	Spiral resonant cell
[51]	0.9	3^{rd}	NA	36	0.325	Power divider	Complementary split ring resonator
[52]	1	2^{nd} to 4^{th}	32	40	0.25	Power divider	Controllable transmission zeros
[53]	1	—	25	20	0.5	Coupler	Fractal resonators
[54]	26	—	11	11	1	Coupler	Dielectric constant
[55]	0.9	2^{nd} and 3^{rd}	28	28	0.3	Coupler	Open stubs
[56]	0.9	3^{rd} and 5^{th}	31	36	0.3	Coupler	Resonant cell
[57]	3	2^{nd} to 4^{th}	23	23	0.4	Coupler	Nonuniform lines
This work	1	3^{rd} to 14^{th}	22.5	21	0.4	Coupler	Elliptic filter and ANN

parameters of the designed coupler, such as isolation and return loss are desirable.

4. Conclusion

This paper presents a novel approach to address the problem of harmonic suppression in microwave coupler applications, particularly in QHCs. The key contributions of this work include the incorporation of simple elliptic LPFs, a radial resonator, and a rectangular resonator into the QHC structure, as well as the utilization of neural networks for device design optimization. Previous approaches to harmonic suppression often involved complex structures, such as EBG and DGS configurations, which could complicate the coupler design. However, this paper introduces an effective approach by integrating simple LPFs directly into the conventional coupler structure. This innovative strategy leads to a significant improvement in coupler performance, particularly in terms of harmonic suppression. The filters are designed using both rectangular-shaped and radial-shaped resonators. Furthermore, neural networks are employed to optimize the LPF design, resulting in enhanced performance and sharper transition bands. Also, the proposed device structure is analyzed and the LC equivalent circuit and its transfer function is extracted. The proposed filter has cut-off frequency of 2.2 GHz, stop-band bandwidth of 10.24 GHz with more than 20 dB suppression level. The proposed LPF provides very sharp response of 158.3 dB/GHz. The impedance analysis of the circuit further validates the simulation results. The conventional QHC design is analyzed and compared with the results of the proposed device. The results of the proposed coupler are desirable, which the simulated S-parameters are close to the desired ideal values. A wide suppression band from 2.25 GHz up to more than 14 GHz effectively addresses the issue of harmonics, providing desirable harmonic suppression for higher-order harmonics. The results of the proposed QHC and its performances are compared with similar devices, which show desirable results of the proposed device.

Data Availability

All data generated or analyzed during this study are included in this published article.

Conflicts of Interest

The authors declare that they have no conflicts of interest.

References

[1] D. Ahn, J.-S. Park, C.-S. Kim, J. Kim, Y. Qian, and T. Itoh, "A design of the low-pass filter using the novel microstrip defected ground structure," *IEEE Transactions on Microwave Theory and Techniques*, vol. 49, no. 1, pp. 86–93, 2001.

[2] J. Karki, "Active Low-Pass Filter Design," Texas Instruments application report, Texas Instruments, TX, USA, 2000.

[3] J.-S. Lim, C.-S. Kim, D. Ahn, Y.-C. Jeong, and S. Nam, "Design of low-pass filters using defected ground structure," *IEEE Transactions on Microwave Theory and Techniques*, vol. 53, no. 8, pp. 2539–2545, 2005.

[4] S. Lotfi, S. Makki, and S. Majidifar, "Design of microstrip lowpass filter with ultra-wide stopband and sharp rejection," *International Journal of Engineering and Technology Sciences (IJETS)*, vol. 2, pp. 47–57, 2014.

[5] S. Roshani, S. I. Yahya, Y. Y. Ghadi, S. Roshani, F. Parandin, and B. D. Yaghouti, "Size reduction and harmonics suppression in microwave power dividers," *ARO-THE SCIENTIFIC JOURNAL OF KOYA UNIVERSITY*, vol. 11, no. 2, pp. 122–136, 2023.

[6] M. A. Chaudhary, S. Roshani, and S. Roshani, "An ultra compact microstrip branch line coupler with wide stopband using LCL filter and meandered stubs for microwave applications," *Processes*, vol. 11, no. 5, p. 1582, 2023.

[7] S. Roshani, S. I. Yahya, Y. S. Mezaal et al., "A compact filtering coupler with unwanted harmonic rejection using LC composite lines for communication systems applications," *Systems*, vol. 11, no. 1, p. 14, 2022.

[8] S. I. Yahya, S. Roshani, M. Ami, Y. Y. Ghadi, M. A. Chaudhary, and S. Roshani, "A compact rat-race coupler with harmonic suppression for GSM applications: design and implementation using artificial neural network," *Micromachines*, vol. 14, no. 7, p. 1294, 2023.

[9] K.-O. Sun, S.-J. Ho, C.-C. Yen, and D. Van Der Weide, "A compact branch-line coupler using discontinuous microstrip lines," *IEEE Microwave and Wireless Components Letters*, vol. 15, no. 8, pp. 519-520, 2005.

[10] K.-K. Cheng and F.-L. Wong, "A novel rat race coupler design for dual-band applications," *IEEE Microwave and Wireless Components Letters*, vol. 15, no. 8, pp. 521–523, 2005.

[11] D. M. Pozar, *Microwave Engineering*, John Wiley and Sons, NJ, USA, 2011.

[12] S. Y. Huang and Y. H. Lee, "Compact U-shaped dual planar EBG microstrip low-pass filter," *IEEE Transactions on Microwave Theory and Techniques*, vol. 53, no. 12, pp. 3799–3805, 2005.

[13] J. Park, J.-P. Kim, and S. Nam, "Design of a novel harmonic-suppressed microstrip low-pass filter," *IEEE Microwave and Wireless Components Letters*, vol. 17, no. 6, pp. 424–426, 2007.

[14] A. B. Abdel-Rahman, A. K. Verma, A. Boutejdar, and A. Omar, "Control of bandstop response of Hi-Lo microstrip low-pass filter using slot in ground plane," *IEEE Transactions on Microwave Theory and Techniques*, vol. 52, no. 3, pp. 1008–1013, 2004.

[15] J. Yang and W. Wu, "Compact elliptic-function low-pass filter using defected ground structure," *IEEE Microwave and Wireless Components Letters*, vol. 18, no. 9, pp. 578–580, 2008.

[16] A. Balalem, A. R. Ali, J. Machac, and A. Omar, "Quasi-elliptic microstrip low-pass filters using an interdigital DGS slot," *IEEE Microwave and Wireless Components Letters*, vol. 17, no. 8, pp. 586–588, 2007.

[17] S. Luo, L. Zhu, and S. Sun, "Stopband-expanded low-pass filters using microstrip coupled-line hairpin units," *IEEE Microwave and Wireless Components Letters*, vol. 18, no. 8, pp. 506–508, 2008.

[18] Z. Mousavirazi, M. M. M. Ali, H. N. Gheisanab, and T. A. Denidni, "Analysis and design of ultra-wideband PRGW hybrid coupler using PEC/PMC waveguide model," *Scientific Reports*, vol. 12, no. 1, 2022.

[19] J.-S. Lim, C.-S. Kim, J.-S. Park, D. Ahn, and S. Nam, "Design of 10 dB 90° branch line coupler using microstrip line with defected ground structure," *Electronics Letters*, vol. 36, no. 21, pp. 1784-1785, 2000.

[20] L. Xia, J.-L. Li, B. A. Twumasi, P. Liu, and S.-S. Gao, "Planar dual-band branch-line coupler with large frequency ratio," *IEEE Access*, vol. 8, pp. 33188–33195, 2020.

[21] A. Bekasiewicz and S. Koziel, "Miniaturised dual-band branch-line coupler," *Electronics Letters*, vol. 51, no. 10, pp. 769–771, 2015.

[22] N. Mohammadi, G. Moloudian, S. Roshani, S. Roshani, F. Parandin, and A. Lalbakhsh, "A Wilkinson power divider with harmonic suppression through low-pass filter for GSM and LTE applications," *Scientific Reports*, vol. 14, no. 1, p. 2429, 2024.

[23] S. Lotfi, S. Roshani, S. Roshani, and M. Shirzadian Gilan, "A planner Doherty power amplifier with harmonic suppression with open and short ended stubs," *Frequenz*, vol. 76, no. 3-4, pp. 121–130, 2022.

[24] H. Zhang and K. J. Chen, "A stub tapped branch-line coupler for dual-band operations," *IEEE Microwave and Wireless Components Letters*, vol. 17, no. 2, pp. 106–108, 2007.

[25] A. Biswas, "Theory of optical couplers," *Optical and Quantum Electronics*, vol. 35, no. 3, pp. 221–235, 2003.

[26] F. Parandin, A. Sheykhian, and N. Bagheri, "A novel design for an ultracompact optical majority gate based on a ring resonator on photonic crystal substrate," *Journal of Computational Electronics*, vol. 22, no. 2, pp. 716–722, 2023.

[27] A. Askarian and F. Parandin, "A novel proposal for all optical 1-bit comparator based on 2D linear photonic crystal," *Journal of Computational Electronics*, vol. 22, pp. 288–295, 2022.

[28] F. Parandin, Z. Rahimi, and M. Rezaeenia, "Design of an ultra-compact photonic crystal based all optical XOR and NOT logic gates," *Journal of Optical Communications*, vol. 0, no. 0, 2022.

[29] M. B. Jamshidi, S. Roshani, J. Talla, M. S. Mohammadi, S. Roshani, and Z. Peroutka, "A modified branch line coupler with ultra-wide harmonics rejection using resonators and open-ended stubs," in *Proceedings of the 2021 IEEE 12th Annual Ubiquitous Computing, Electronics and Mobile Communication Conference (UEMCON)*, pp. 0860–0865, New York, NY, USA, November 2021.

[30] S. Roshani, S. Roshani, M. B. Jamshidi, M. Karimi, and N. Mahtabi, "A dual band microstrip branch line coupler with harmonics suppression using LPF and open ended stubs," in *Proceedings of the 2021 Photonics and Electromagnetics Research Symposium PIERS*, pp. 1597–1604, Hangzhou, China, November 2021.

[31] S. Koziel and A. Bekasiewicz, "Low-cost and reliable geometry scaling of compact microstrip couplers with respect to operating frequency, power split ratio, and dielectric substrate parameters," *IET Microwaves, Antennas and Propagation*, vol. 12, no. 9, pp. 1508–1513, 2018.

[32] J. Coromina, P. Velez, J. Bonache, and F. Martín, "Branch line couplers with small size and harmonic suppression based on non-periodic step impedance shunt stub (SISS) loaded lines," *IEEE Access*, vol. 8, pp. 67310–67320, 2020.

[33] N. Calik, F. Güneş, S. Koziel, A. Pietrenko-Dabrowska, M. A. Belen, and P. Mahouti, "Deep-learning-based precise characterization of microwave transistors using fully-automated regression surrogates," *Scientific Reports*, vol. 13, no. 1, p. 1445, 2023.

[34] M. Roshani, G. Phan, G. Hossein Roshani et al., "Combination of X-ray tube and GMDH neural network as a non-destructive and potential technique for measuring characteristics of gas-oil–water three phase flows," *Measurement*, vol. 168, 2021.

[35] M. Roshani, G. T. Phan, P. Jammal Muhammad Ali et al., "Evaluation of flow pattern recognition and void fraction measurement in two phase flow independent of oil pipeline's scale layer thickness," *Alexandria Engineering Journal*, vol. 60, no. 1, pp. 1955–1966, 2021.

[36] M. Roshani, M. A. Sattari, P. J. Muhammad Ali et al., "Application of GMDH neural network technique to improve measuring precision of a simplified photon attenuation based two-phase flowmeter," *Flow Measurement and Instrumentation*, vol. 75, 2020.

[37] A. Pietrenko-Dabrowska, S. Koziel, and M. Al-Hasan, "Expedited yield optimization of narrow-and multi-band antennas using performance-driven surrogates," *IEEE Access*, vol. 8, pp. 143104–143113, 2020.

[38] S. Koziel and A. Pietrenko-Dabrowska, "Expedited feature-based quasi-global optimization of multi-band antenna input characteristics with jacobian variability tracking," *IEEE Access*, vol. 8, pp. 83907–83915, 2020.

[39] S. Koziel and A. Pietrenko-Dabrowska, "Constrained multi-objective optimization of compact microwave circuits by design triangulation and pareto front interpolation," *European Journal of Operational Research*, vol. 299, no. 1, pp. 302–312, 2022.

[40] F. Parandin and A. Mohamadi, "Designing and optimizing a photonic crystal-based all-optical XOR gate using machine learning," *Majlesi Journal of Electrical Engineering*, 2023.

[41] M. Feli and F. Parandin, "A numerical optimization of an efficient double junction InGaN/CIGS solar cell," *Journal of Electrical and Computer Engineering Innovations*, vol. 6, pp. 53–58, 2017.

[42] M. B. Jamshidi, A. Lalbakhsh, B. Mohamadzade, H. Siahkamari, and S. M. H. Mousavi, "A novel neural-based approach for design of microstrip filters," *AEU-International Journal of Electronics and Communications*, vol. 110, 2019.

[43] A. Lalbakhsh, R. B. Simorangkir, N. Bayat-Makou, A. A. Kishk, and K. P. Esselle, "Advancements and artificial intelligence approaches in antennas for environmental sensing," *Artificial Intelligence and Data Science in Environmental Sensing*, pp. 19–38, 2022.

[44] B. Mahjoob Karambasti, M. Ghodrat, G. Ghorbani, A. Lalbakhsh, and M. Behnia, "Design methodology and multi-objective optimization of small-scale power-water production based on integration of Stirling engine and multi-effect evaporation desalination system," *Desalination*, vol. 526, 2022.

[45] S. Roshani, S. Koziel, S. I. Yahya et al., "Mutual coupling reduction in antenna arrays using artificial intelligence approach and inverse neural network surrogates," *Sensors*, vol. 23, no. 16, p. 7089, 2023.

[46] M. Jamshidi, S. I. Yahya, S. Roshani, M. A. Chaudhary, Y. Y. Ghadi, and S. Roshani, "A fast surrogate model-based algorithm using multilayer perceptron neural networks for microwave circuit design," *Algorithms*, vol. 16, no. 7, p. 324, 2023.

[47] S. I. Yahya, B. M. Alameri, M. Jamshidi et al., "A New Design method for class-E power amplifiers using artificial intelligence modeling for wireless power transfer applications," *Electronics*, vol. 11, no. 21, p. 3608, 2022.

[48] F. Zhang and C. Li, "Power divider with microstrip electromagnetic bandgap element for miniaturisation and harmonic rejection," *Electronics Letters*, vol. 44, no. 6, pp. 422–424, 2008.

[49] J. He, Z. Feng Chen, B. Hai Yang, and M. Ying Xiong, "Miniaturized microstrip Wilkinson power divider with

capacitor loading," *Microwave and Optical Technology Letters*, vol. 54, no. 1, pp. 61–63, 2012.

[50] J. Gu and X. Sun, "Miniaturization and harmonic suppression rat-race coupler using C-SCMRC resonators with distributive equivalent circuit," *IEEE Microwave and Wireless Components Letters*, vol. 15, no. 12, pp. 880–882, 2005.

[51] S. Karthikeyan and R. Kshetrimayum, "Compact, harmonic suppressed power divider using open complementary split-ring resonator," *Microwave and Optical Technology Letters*, vol. 53, no. 12, pp. 2897–2899, 2011.

[52] K.-K. M. Cheng and W.-C. Ip, "A novel power divider design with enhanced spurious suppression and simple structure," *IEEE Transactions on Microwave Theory and Techniques*, vol. 58, pp. 3903–3908, 2010.

[53] A. Tayebi and D. Zarifi, "On the miniaturization of microstrip ring-hybrid couplers using Gielis supershapes," *IETE Journal of Research*, vol. 69, no. 2, pp. 1160–1165, 2023.

[54] N. A. Mohd Shukor and N. Seman, "5G planar branch line coupler design based on the analysis of dielectric constant, loss tangent and quality factor at high frequency," *Scientific Reports*, vol. 10, no. 1, 2020.

[55] I. S. Krishna, R. K. Barik, S. Karthikeyan, and P. Kokil, "A miniaturized harmonic suppressed 3 dB branch line coupler using H-shaped microstrip line," *Microwave and Optical Technology Letters*, vol. 59, no. 4, pp. 913–918, 2017.

[56] S. Roshani and S. Roshani, "A compact coupler design using meandered line compact microstrip resonant cell (MLCMRC) and bended lines," *Wireless Networks*, vol. 27, no. 1, pp. 677–684, 2021.

[57] K. A. Alshamaileh, V. K. Devabhaktuni, and N. I. Dib, "Impedance-varying broadband 90° branch-line coupler with arbitrary coupling levels and higher order harmonic suppression," *IEEE Transactions on Components, Packaging, and Manufacturing Technology*, vol. 5, no. 10, pp. 1507–1515, 2015.